Commensurability oscillations by snake-orbit magnetotransport in two-dimensional electron gases

A. Leuschner, J. Schluck, M. Cerchez,* and T. Heinzel
Solid State Physics Laboratory, Heinrich-Heine-Universität Düsseldorf, 40204 Düsseldorf, Germany

K. Pierz and H. W. Schumacher
Physikalisch-Technische Bundesanstalt, Bundesallee 100, D-38116 Braunschweig, Germany
(Received 25 January 2017; revised manuscript received 3 April 2017; published 24 April 2017)

Commensurate magnetoresistance periodic oscillations generated by transversal electron snake orbits are found experimentally. A two-dimensional electron gas is exposed to a magnetic field that changes sign along the current longitudinal direction and is homogeneous in the transverse direction. The change in sign of the magnetic field directs the electron flow along the transversal direction, in snake orbits. This generates resistance oscillations with a predictable periodicity that is commensurate with the width of the electron gas. Numerical simulations are used to reveal the character of the oscillations.

DOI: 10.1103/PhysRevB.95.155440

I. INTRODUCTION

Magnetotransport phenomena in magnetic fields localized at least in one direction have been reported for some time, and the interest has been both at the fundamental and application levels [1]. Various magnetic field profiles led to effects such as commensurate oscillations [2,3], a giant magnetoresistance [4], and snake-orbit dominated transport [5]. Also magnetic wave guiding of electrons [6], resistance oscillations at magnetic edge states [7], detection of spin resonance by electron channeling along snake orbits [8], and snake-orbit induced rectification [9] were reported. Magnetic barriers, i.e., localized magnetic fields in the direction of the current which are homogeneous in the transverse direction, have been studied in great detail [10–17], and typically show a smooth magnetoresistance which is influenced by both momentum-randomizing scattering in the bulk and $\vec{E} \times \vec{B}$ drift at the sample edges [18]. Inhomogeneous magnetic fields in quantum wires, on the other hand, show phenomena such as transmission and reflection resonances [19] and can host quantum states which have no semiclassical analog [20–22]. Two-dimensional electron gases (2DEGs) exposed to inhomogeneous magnetic fields raise application interest in particular in relation to Hall magnetometry on magnetic micro- or nanostructures [23–29] and to solid-state spin filters [30–35]. More recently, localized magnetic fields at quantum dots were used to manipulate single spins [36,37] and to demonstrate electrical control of a spin qubit [38]. In applications such as these, it is potentially important to develop a thorough understanding of the possible magnetotransport outcome that the magnetic field profile may generate.

In the general effort of understanding and exploiting the potential of localized magnetic fields, this paper reports the observation of magnetoresistance periodic oscillations in localized magnetic fields, which are due to transverse electron snake orbits commensurate with the spatial extension of the 2DEG. The interpretation of the experimental results is based on classical and quantum simulations showing, through classical electron trajectories as well as the electron local density of states, how the transversal snake-orbit electron transport is responsible for the magnetoresistance oscillations.

Section II describes the geometry and preparation of the samples. The experimental results and their interpretation are presented in Sec. III. The paper closes with conclusions in Sec. IV.

II. SAMPLE PREPARATION, EXPERIMENTAL SETUP, AND CHARACTERIZATION MEASUREMENTS

The samples were prepared from two $GaAs/Al_{0.3}Ga_{0.7}As$ heterostructures (samples A and B). The 2DEG in sample A is located $d = 150$ nm below the surface and had, after illumination with an infrared light-emitting diode for a few seconds, an electron density of $n = 2.7 \times 10^{15}$ m^{-2} and a mobility of $\mu = 168$ m^2/Vs at a temperature of $\approx$100 mK. The corresponding values for sample B were $d = 90$ nm, $n = 3.5 \times 10^{15}$ m^{-2}, and $\mu = 131$ m^2/Vs. Optical lithography and wet chemical etching were used to define a Hall bar of $w = 10$ μm width in the y direction. This is smaller than the mean free path of 14 μm in sample A and 12 μm in sample B, such that the electrons could cross the Hall bar ballistically. After covering the surface with a Cr film of 5 nm thickness, a ferromagnetic Dy platelet with a thickness of $h = 250$ nm was deposited by thermal evaporation in a vacuum chamber. Finally, the samples were covered by a Cr/Au gate that protects the Dy from oxidation and could be used to tune the electron density.

The experiments were carried out at an electron temperature of $T \approx 100$ mK in a dilution refrigerator, equipped with a 12 T superconducting magnet. The sample holder had a rotatable stage such that the sample could be oriented with respect to the magnetic field by rotation about the y axis. The Dy film was magnetized by applying an in-plane magnetic field $B_\parallel$ in the transport (x) direction. The 2DEG responds predominantly to the perpendicular magnetic field $B_z(x)$ via the Lorentz force. Effects due to in-plane magnetic fields and to spin splitting were much weaker and are neglected in the following. The perpendicular magnetic field in the plane of the 2DEG close to $x = 0$ in the configuration shown in Figs. 1(a) and 1(b) is

*mihai.cerchez@hhu.de

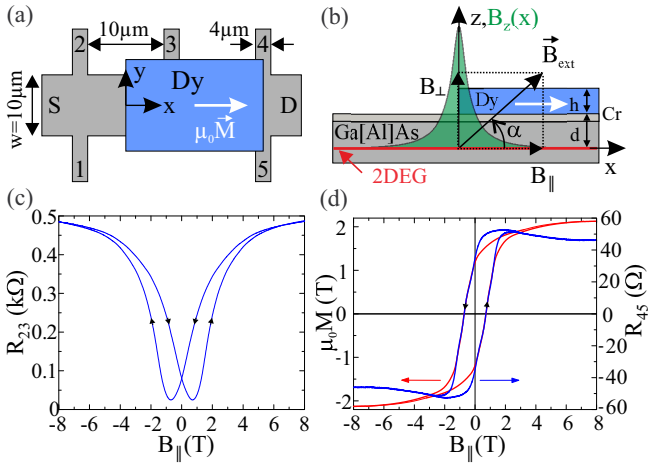

FIG. 1. (a) Top-view scheme of the sample layout. The Dy film is magnetized in the transport direction, creating a localized magnetic field profile under the edges. The homogeneous Cr/Au gate that covers the whole structure is not shown. (b) Sketch of the sample orientation with respect to the magnetic field $\vec{B}_{ext}$ generated by the superconducting magnet. (c) Longitudinal resistance of the magnetic barrier as a function of $B_\parallel$ for parallel alignment of the sample. Arrows indicate the sweep direction. (d) The barrier's Hall resistance (blue) and the extracted magnetization trace of the Dy film (red).

given by [15]

$$B_z(x,B_x) = B_\perp - \frac{\mu_0 M(B_x)}{4\pi} \ln\left[\frac{x^2+d^2}{x^2+(d+h)^2}\right], \qquad (1)$$

where $B_\perp$ denotes the homogeneous component that was tuned by rotating the sample. The second term originates from the fringe field generated by the Dy platelet. This structure is usually denoted as *magnetic barrier* and has an approximately Lorentzian shape with a full width at half maximum of $2\sqrt{d(d+h)}$, which amounted to 420 nm for sample A and 350 nm for sample B. At our maximum Dy magnetization of $\mu_0 M_s = 2.1$ T (see below), its peak reaches values as high as 370 mT for sample A and 440 mT for sample B, respectively. Consequently, magnetic field gradients of the order of 2×10^6 Tm^{-1} can be generated by magnetic barriers in 2DEGs. Offsetting the magnetic barrier by applying $B_\perp$ of opposite sign thus forces the electrons on snake trajectories, oriented in the y direction along the roots of $B_z(x,B_x)$. This concept is used in the following to generate and tune snake trajectories. As shown in Fig. 1(a), one edge of the Dy platelet resides in between contacts 2 and 3. This allows studies of the longitudinal magnetoresistance R_{xx} produced by the corresponding magnetic texture. The opposite edge is located inside contacts 4 and 5 in order to measure the Hall voltage generated by the magnetic barrier and thereby to determine the magnetization of the Dy film.

Rotating the sample about the y axis by small angles $\alpha \leqslant 3^\circ$ with respect to the parallel configuration, in a magnetic field of 10 T, allows the saturation magnetization to remain in the x-y plane to a very good approximation (99.8%), while $B_\perp$ with strengths up to the order of the magnetic barrier amplitude can be added [39]. A scheme of the rotated sample is shown in Fig. 1(b).

An ac current of 50 nA amplitude and with a frequency of 37 Hz is maintained through the sample. The Dy film and the magnetic barrier are characterized by resistance measurements in applied parallel magnetic fields; see Fig. 1(c). The longitudinal magnetoresistance R_{23} shows the typical hysteretic $B_\parallel$ dependence of magnetic barriers [14,15]. In our sample, the relative increase of the magnetic barrier resistance of more than a factor of 20 is quite large, which can be traced back to the small rate of elastic scattering that promotes transmission through the barrier [18]. The large ballisticity of our samples is also reflected in the Hall resistance $R_{45}(B_\parallel)$, which shows a characteristic maximum at intermediate magnetic fields ($B_\parallel = 2.2$ T for the up-sweep). It has been shown recently that this structure is due to a ballistic focusing effect, but the Hall voltage may nevertheless be used to determine the Dy film magnetization [40,41], which for our samples gives the magnetization trace shown in Fig. 1(d). It saturates for $B_\parallel \geqslant 7$ T at a value of $\mu_0 M_s = 2.1$ T. Furthermore, we have studied the Hall resistance as a function of α up to $\alpha = 3^\circ$ and confirmed that the homogeneous perpendicular component $B_\perp$ in this interval is a simple superposition to the magnetic barrier field, in agreement with findings reported earlier [39].

III. RESULTS AND DISCUSSIONS

In order to study the effects of $B_\perp$, the external magnetic field is set to $B_{ext} = 10$ T and R_{23} is measured as a function of the rotation angle α. The Hall voltage between probes 1 and 2 was simultaneously recorded and was used to determine $B_\perp$. The results are shown in Fig. 2, where $R_{23}(B_\perp)$ is plotted for both samples and as a function of the electron density. In sample A [Fig. 2(a)], up to three resistance peaks are observed on top of a smoothly varying background in the interval where $B_\perp$ is antiparallel to the magnetic barrier ($\alpha < 0$ in Fig. 1) but of smaller amplitude. The peak positions shift slightly towards more negative values of $B_\perp$ as n is increased, while their amplitude is most pronounced for slightly negative gate voltages, around electron densities of 2.4×10^{15} m^{-2}. Furthermore, the amplitude tends to decrease as $B_\perp$ becomes more negative. We note that the tuning range of n is quite limited, a well-known problem in high-mobility heterostructures which has been traced back to hysteresis effects [42]. In addition, one resistance peak is observed in the interval where $B_\perp$ and the magnetic barrier are coparallel (for positive values of $B_\perp$). Similar features are observed in sample B, where the background resistance has a different shape, while the peak at coparallel alignment is absent. A corresponding experiment in the quasidiffusive regime where the mean free path was smaller than w has been carried out by Hugger *et al.* [39]. In that experiment, a magnetoresistance with a similar smooth variation was observed and could be explained by competing contributions of snake and cycloid orbits in the y direction, in combination with $\vec{E} \times \vec{B}$ drifts at the sample edges. However, the periodic oscillations reported in this work were absent in that experiment. The appearance of these oscillations in the range of $B_\perp$ where $B_z(x)$ changes its sign suggests that they may be related to electron transport along snake trajectories, which are oriented in the y direction, along the roots of $B_z(x)$.

We proceed by interpreting the origin of the oscillations with guidance from numerical simulations. Semiclassical

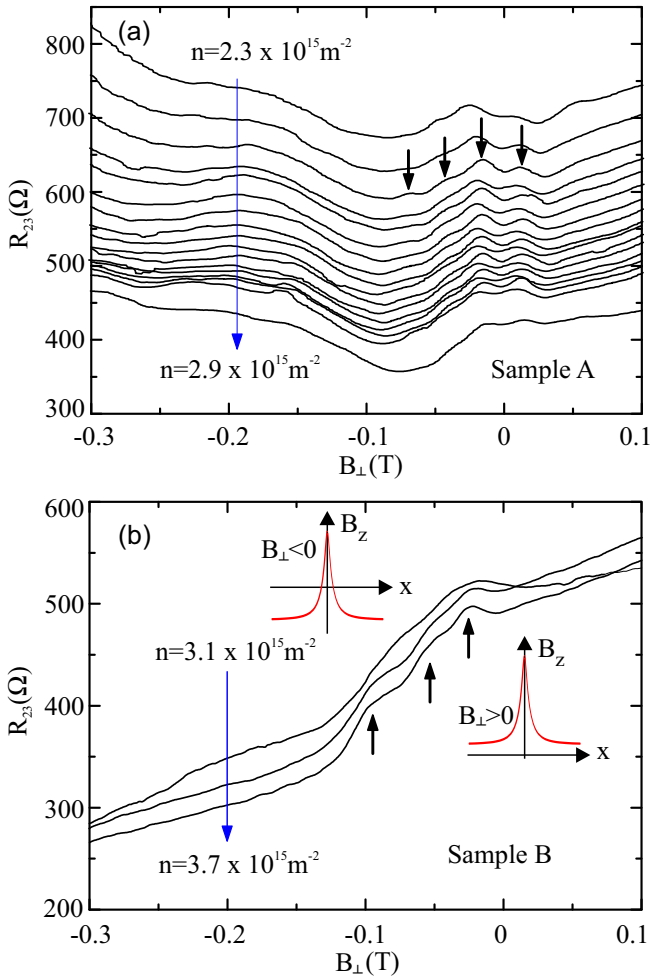

FIG. 2. $R_{23}(B_\perp)$ for samples (a) A and (b) B for different electron densities, with the Dy film at saturation magnetization. The insets in (b) sketch $B_z(x)$ (red) for positive and negative $B_\perp$.

simulations are carried out within the Landauer-Büttiker formalism [43], in the ballistic limit [44]. Electrons are treated as point particles and injected at the Fermi energy in a four-probe geometry with parameters identical to those of sample B, and the magnetoresistance components are calculated as described in detail elsewhere [39]. In Fig. 3, the results of the simulation (trace b) are compared to the experimental trace. Five magnetoresistance peaks are found for the antiparallel alignment of the magnetic barrier and $B_\perp$, and an additional peak is observed for the coparallel alignment very close to $B_\perp = 0$. The positions of peaks 1 to 3 agree reasonably well with the measurements, while peaks 4 and 5 are not observed experimentally. This is due to the effect of scattering which is absent in simulations. For $B_\perp < -0.2$ T, no further oscillations appear and a smooth, almost constant magnetoresistance is found.

These simulations show that the oscillations have a classical character. By inspection of the calculated trajectories, it is conceptually possible to find characteristic orbits that move along the y direction at the magnetoresistance maxima for $B_\perp < 0$. If $B_z(x)$ has no sign change and the magnetic barrier is closed, electrons in the bulk are reflected, but transmission is still possible by $\vec{E} \times \vec{B}$ drifts at the Hall bar edges. As was

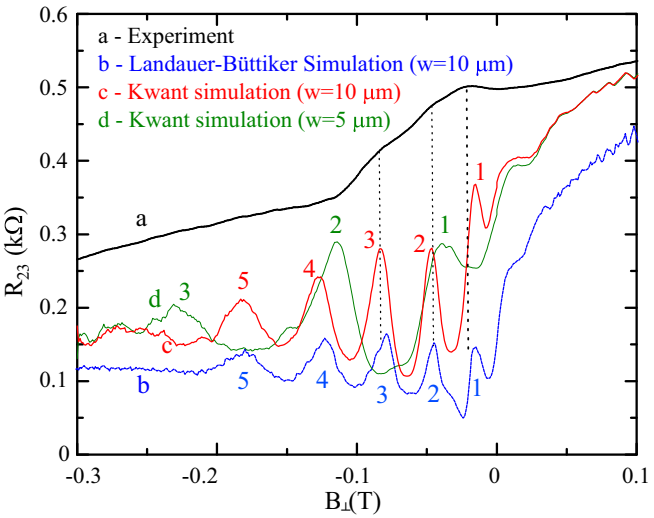

FIG. 3. Experimental data from sample B in comparison with the semiclassical and the quantum simulations, for the electron density $n = 3.5 \times 10^{15}$ m^{-2}. The dotted lines indicate the position of the oscillations that are visible in the experimental curve (corresponding to peaks 1, 2, and 3).

already shown in Ref. [39], by superimposing $B_\perp$ with opposite orientation to the magnetic barrier, two lines of zero field along the y direction are generated, and the $\vec{E} \times \vec{B}$ drift at one edge changes sign, thereby suppressing the edge transmission. On the other hand, this structure can enable a guided transfer of electrons from one Hall bar edge to the other, where they either pass the barrier or are reflected, depending on the exact position and angle at which the electrons hit the edge.

To understand the relevance of this interplay for the oscillatory behavior, one needs either to look at classical trajectories from a statistical point of view in the classical picture or calculate the local density of states (LDOS) in the barrier region within a quantum mechanical treatment which, for sufficiently many occupied states, should be interpretable in terms of classical trajectories.

In the following, we opt for the second possibility and show that the oscillations can be interpreted in a straightforward way with the help of the local density of states. We use the KWANT package [45] for the implementation of the quantum simulations, where again the geometry (with slight modifications for the contacts) and parameters of sample B form the starting point [46]. Electron waves enter the Hall bar via the leads formed by contacts S, 1, and 2 in Fig. 1(a). The tight-binding model is used to calculate the electronic wave functions inside the Hall bar, the resulting local density of states (LDOS), as well as the longitudinal resistance R_{23}. The results (trace c in Fig. 3) agree well with those of the classical simulations, thereby supporting the view that quantum aspects are of minor relevance. The oscillation amplitude in the quantum simulation is larger compared to the classical one, which is most likely due to elastic scattering which is included in the Landauer-Büttiker model, but not in the quantum simulation. In Fig. 4, the local density of states is shown for the states that are occupied by electron injection from contacts S, 1, and 2 for selected values of $B_\perp$. For $B_\perp = -48$ mT [Fig. 4(a)], R_{23} is at the maximum

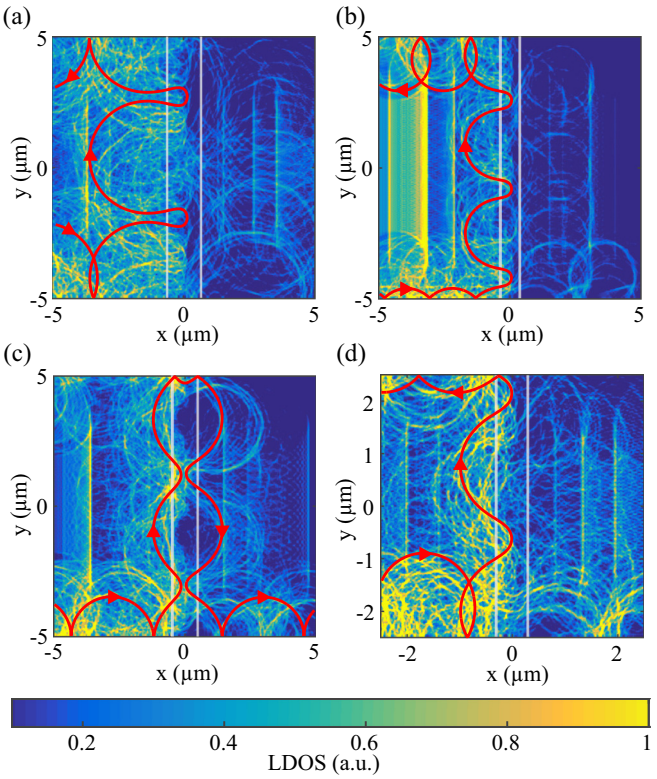

FIG. 4. Local density of states at the maxima of resistance peaks (a) 2 and (b) 3 as well as at the minimum in between (c) for the experimentally implemented structure with a Hall bar width of 10 μm, and (d) for the maximum of resistance peak 2 in a 5-μm-wide Hall bar. In each case, the electron motion is exemplified by a corresponding classical trajectory (red lines with arrows). Also, the zero lines of the perpendicular magnetic field $B - z(x)$ are denoted by the semitransparent gray lines.

of peak 2. Since this magnetic field is chosen to point in the $-z$ direction, the electrons move towards the magnetic barrier preferably via the lower edge of the Hall bar due to $\vec{E} \times \vec{B}$ drift, are reflected at the barrier with a large probability, and move towards contact 2 along the upper Hall bar edge. Close to the magnetic barrier, the LDOS develops a localized shape which we interpret as the superposition of electronic waves that form snake trajectories.

For an illustration of this interpretation, a calculated classical representative trajectory is superimposed to the LDOS. In this picture, the electrons leave the lower sample edge within one cyclotron radius from the magnetic barrier, but still some distance away from the root of the magnetic profile. They move in the $+y$ direction via snake trajectories that are quasicommensurate with the width of the Hall bar, i.e., their period is approximately $w/2$ in this particular case. Due to this commensurability, the electrons hit the upper edge also at a relatively large distance from the magnetic barrier to its left side, which ensures backscattering towards lead 2.

This pattern reappears qualitatively at the peak of oscillation 3 [$B_\perp = -85$ mT, Fig. 4(b)]. Here, the snake trajectory shows a period of $w/3$. The LDOS for $B_\perp = -65$ mT, at the resistance minimum between peaks 2 and 3, is shown in Fig. 4(c). Again, a snake trajectory along the magnetic barrier is visible, but it is incommensurate with w. The small LDOS at the upper left edge of the Hall bar and the increased one at the lower right edge agree with the reduced backscattering and the increased transmission. Here, the fact that approximately 2.5 snake-trajectory periods fit in the Hall bar ensures that many electrons occupying the snake trajectories hit the upper Hall bar in the interval where $B_z > 0$, and they therefore cross the magnetic barrier. We have also calculated the magnetoresistance for the same magnetic structure in a Hall bar with smaller width of $w = 5$ μm (trace d in Fig. 3). Within the commensurability picture, resistance peak 2 (Fig. 3) is attributed to approximately two snake periods across the Hall bar. This oscillation is thus shifted to a more negative value of $B_\perp$, i.e., to -115 mT. The corresponding LDOS at this peak position is reproduced in Fig. 4(d), where again quasicommensurate snake orbits can be identified. We emphasize that further trajectories, such as cycloid and incommensurate snake orbits, do exist for all magnetic fields. However, the LDOS suggests that they contribute with a lower weight to the oscillations. Within this picture, it furthermore becomes apparent why the oscillations disappear for more negative values of $B_\perp$. The zeros of $B_z(x)$ approach the center of the magnetic barrier and finally vanish, together with the snake orbits, as $B_z(x)$ becomes unipolar.

Finally, we comment on the peak observed in the absence of a sign change of $B_z(x)$ at sample A [first marked peak on the right-hand side in Fig. 2(a)]. This peak appears in the simulations very close to $B_\perp = 0$ on top of a strongly increasing background. While it is clear that this peak must have a different character than those due to the snake-orbit electron motion, we could not identify characteristic trajectories. Comparing the quantum simulations for $w = 10$ and 5 μm, we notice that this peak does not change its position. This suggests that it does not originate from a commensurability effect of some orbit across the Hall bar, but may be due to noncommensurate cycloid orbits or related to the sharply changing $\vec{E} \times \vec{B}$ drift at the intersections of the magnetic barrier with the Hall bar edges.

IV. CONCLUSIONS

We have observed commensurability oscillations in two-dimensional electron gases exposed to an inhomogeneous magnetic field in the transport direction, which is translationally invariant in the transverse direction. For magnetic field profiles with two sign changes in series, resistance oscillations are observed as a function of the homogeneous magnetic field component. Based on our simulations, we interpret the resistance oscillations as dominated by snake-orbit enhanced backscattering, an effect which is particularly strong when the snake trajectories are commensurate with the Hall bar in the sense that the Hall bar width is a multiple integer of the snake-trajectory period.

The effect can thus be interpreted in classical terms, in contrast to the resonances in a magnetic field profile with a single sign change. The observation is based on electrons that cross the Hall bar ballistically in the transverse direction. Therefore, the conditions for the width of the Hall bar are quite stringent, since on the other hand in the implementation presented here, the period of the snake orbit cannot be made much smaller than about 2 μm due to the available magnetic barrier amplitudes. A comparison of the simulated amplitudes to the experimental

ones also suggests that unknown imperfections, such as inhomogeneities of the magnetic barrier or additional diffusive scattering at the edge of the Hall bar, have some influence on the visibility of these commensurability oscillations.

ACKNOWLEDGMENTS

The authors thank Professor Phil Bissell for reading the manuscript and HHU Düsseldorf for financial support.

[1] A. Nogaret, J. Phys. Condens. Matter **22**, 253201 (2010).
[2] P. D. Ye, D. Weiss, R. R. Gerhardts, M. Seeger, K. von Klitzing, K. Eberl, and H. Nickel, Phys. Rev. Lett. **74**, 3013 (1995).
[3] H. A. Carmona, A. K. Geim, A. Nogaret, P. C. Main, T. J. Foster, M. Henini, S. P. Beaumont, and M. G. Blamire, Phys. Rev. Lett. **74**, 3009 (1995).
[4] A. Nogaret, S. Carlton, B. L. Gallagher, P. C. Main, M. Henini, R. Wirtz, R. Newbury, M. A. Howson, and S. P. Beaumont, Phys. Rev. B **55**, R16037(R) (1997).
[5] J. Schluck, S. Fasbender, T. Heinzel, K. Pierz, H. W. Schumacher, D. Kazazis, and U. Gennser, Phys. Rev. B **91**, 195303 (2015).
[6] A. Nogaret, D. N. Lawton, D. K. Maude, J. C. Portal, and M. Henini, Phys. Rev. B **67**, 165317 (2003).
[7] A. Nogaret, S. J. Bending, and M. Henini, Phys. Rev. Lett. **84**, 2231 (2000).
[8] A. Nogaret, F. Nasirpouri, J.-C. Portal, H. E. Beere, D. A. Ritchie, A. T. Hindmarch, and C. H. Marrows, Europhys. Lett. **94**, 28001 (2011).
[9] M. Hara, A. Endo, S. Katsumoto, and Y. Iye, Phys. Rev. B **69**, 153304 (2004).
[10] F. M. Peeters and A. Matulis, Phys. Rev. B **48**, 15166 (1993).
[11] A. Matulis, F. M. Peeters, and P. Vasilopoulos, Phys. Rev. Lett. **72**, 1518 (1994).
[12] F. G. Monzon, M. Johnson, and M. L. Roukes, Appl. Phys. Lett. **71**, 3087 (1997).
[13] M. Johnson, B. R. Bennett, M. J. Yang, M. M. Miller, and B. V. Shanabrook, Appl. Phys. Lett. **71**, 974 (1997).
[14] V. Kubrak, A. Neumann, B. L. Gallagher, P. C. Main, M. Henini, C. H. Marrows, and B. J. Hickey, J. Appl. Phys. **87**, 5986 (2000).
[15] T. Vančura, T. Ihn, S. Broderick, K. Ensslin, W. Wegscheider, and M. Bichler, Phys. Rev. B **62**, 5074 (2000).
[16] B. L. Gallagher, V. Kubrak, A. W. Rushforth, A. C. Neumann, K. W. Edmonds, P. C. Main, M. Henini, C. H. Marrows, B. J. Hickey, and S. Thoms, Physica E (Amsterdam) **11**, 171 (2001).
[17] V. Kubrak, K. W. Edmonds, A. C. Neumann, B. L. Gallagher, P. C. Main, M. Henini, C. H. Marrows, B. J. Hickey, and S. Thoms, IEEE Trans. Magn. **37**, 1992 (2001).
[18] M. Cerchez, S. Hugger, T. Heinzel, and N. Schulz, Phys. Rev. B **75**, 035341 (2007).
[19] A. Tarasov, S. Hugger, H. Xu, M. Cerchez, T. Heinzel, I. V. Zozoulenko, U. Gasser-Szerer, D. Reuter, and A. D. Wieck, Phys. Rev. Lett. **104**, 186801 (2010).
[20] J. Reijniers, A. Matulis, K. Chang, F. M. Peeters, and P. Vasilopoulos, Europhys. Lett. **59**, 749 (2002).
[21] H. Xu, T. Heinzel, M. Evaldsson, S. Ihnatsenka, and I. V. Zozoulenko, Phys. Rev. B **75**, 205301 (2007).
[22] B. Schüler, M. Cerchez, H. Xu, J. Schluck, T. Heinzel, D. Reuter, and A. D. Wieck, Phys. Rev. B **90**, 201111(R) (2014).
[23] A. K. Geim, I. V. Grigorieva, S. V. Dubonos, J. G. S. Lok, J. C. Maan, A. E. Filippov, and F. M. Peeters, Nature (London) **390**, 259 (1997).
[24] A. K. Geim, S. V. Dubonos, J. G. S. Lok, I. V. Grigorieva, J. C. Maan, L. T. Hansen, and P. E. Lindelof, Appl. Phys. Lett. **71**, 2379 (1997).
[25] F. M. Peeters and X. Q. Li, Appl. Phys. Lett. **72**, 572 (1998).
[26] S. Pedersen, G. R. Kofod, J. C. Hollingbery, C. B. Sørensen, and P. E. Lindelof, Phys. Rev. B **64**, 104522 (2001).
[27] K. S. Novoselov, A. K. Geim, S. V. Dubonos, Y. G. Cornelissens, F. M. Peeters, and J. C. Maan, Phys. Rev. B **65**, 233312 (2002).
[28] K. S. Novoselov, A. K. Geim, S. V. Dubonos, E. W. Hill, and I. V. Grigorieva, Nature (London) **426**, 812 (2003).
[29] G. Mihailovic, A. Hoffmann, and S. von Molnar, J. Appl. Phys. **106**, 074518 (2009).
[30] A. Majumdar, Phys. Rev. B **54**, 11911 (1996).
[31] Y. Guo, B.-L. Gu, Z. Zeng, J.-Z. Yu, and Y. Kawazoe, Phys. Rev. B **62**, 2635 (2000).
[32] G. Papp and F. M. Peeters, Appl. Phys. Lett. **78**, 2184 (2001).
[33] G. Papp and F. M. Peeters, Appl. Phys. Lett. **79**, 3198 (2001).
[34] H. Z. Xu and Y. Okada, Appl. Phys. Lett. **79**, 3119 (2001).
[35] F. Zhai and H. Q. Xu, Appl. Phys. Lett. **88**, 032502 (2006).
[36] M. Pioro-Ladriére, T. Obata, Y. Tokura, Y.-S. Shin, T. Kubo, K. Yoshida, T. Taniyama, and S. Tarucha, Nat. Phys. **4**, 776 (2008).
[37] K. C. Nowack, F. H. L. Koppens, Y. V. Nazarov, and L. M. K. Vandersypen, Science **318**, 1430 (2007).
[38] E. Kawakami, P. Scarlino, D. R. Ward, F. R. Braakman, D. E. Savage, M. G. Lagally, M. Friesen, S. N. Coppersmith, M. A. Eriksson, and L. M. K. Vandersypen, Nat. Nano **9**, 666 (2014).
[39] S. Hugger, M. Cerchez, H. Xu, and T. Heinzel, Phys. Rev. B **76**, 195308 (2007).
[40] S. Fasbender, J. Schluck, M. Cerchez, T. Heinzel, S. Sievers, K. Pierz, and H. W. Schumacher, J. Appl. Phys. **119**, 094302 (2016).
[41] M. Cerchez and T. Heinzel, Appl. Phys. Lett. **98**, 232111 (2011).
[42] C. Rüssler, T. Feil, P. Mensch, T. Ihn, K. Ensslin, D. Schuh, and W. Wegscheider, New J. Phys. **12**, 043007 (2010).
[43] M. Büttiker, Phys. Rev. Lett. **57**, 1761 (1986).
[44] C. W. J. Beenakker, Phys. Rev. Lett. **62**, 2020 (1989).
[45] C. W. Groth, M. Wimmer, A. R. Akhmerov, and X. Waintal, New J. Phys. **16**, 063065 (2014).
[46] H. U. Baranger and A. D. Stone, Phys. Rev. Lett. **63**, 414 (1989).